Semiconductor Physics, Quantum Electronics & Optoelectronics, 2021. V. 24, No 2. P. 185-191.

Optoelectronics and optoelectronic devices

Spintronics phenomena induced by THz radiation in narrow-gap HgCdTe thin films in an external constant electric field

Z.F. Tsybrii[1*], S.N. Danilov[2], J.V. Gumenjuk-Sichevska[1], N.N. Mikhailov[3], S.A. Dvoretskii[3,4], E.O. Melezhik[1], F.F. Sizov[1]

[1]*V. Lashkaryov Institute of Semiconductor Physics, NAS of Ukraine, 41, prosp. Nauky, 03680 Kyiv, Ukraine*
[2]*Terahertz Center, University of Regensburg, 93040 Regensburg, Germany*
[3]*Rzhanov Institute of Semiconductor Physics of the Siberian Branch of the RAS, 13, Ac. Lavrentieva ave., Novosibirsk, Russia, 630090, Russian Federation*
[4]*Tomsk State University, Tomsk 634050, Russian Federation*
**Corresponding author e-mail: tsybrii@isp.kiev.ua*

Abstract. The responses of uncooled (T = 300 K) and cooled to T = 78 K antenna-coupled $Hg_{1-x}Cd_xTe$-based narrow-gap thin-film photoconductors having large spin-orbit coupling and irradiated by the terahertz (THz) radiation (linearly or circularly polarized) have been investigated. Powerful THz radiation excitation causes photocurrents, which signs and magnitudes are controlled by orientation of antenna axes, an external constant electric field direction and orientation of the polarized (circular or linear) radiation electric field falling onto photoconductors. The observed effects seem to be caused by the spin currents observed in devices where spintronic effects are revealed.

Keywords: spintronic phenomena, photoconductors, THz radiation, HgCdTe.

https://doi.org/10.15407/spqeo24.02.185
PACS 73.50.Pz, 73.61.Ga, 85.75.-d

Manuscript received 22.04.21; revised version received 11.05.21; accepted for publication 02.06.21; published online 16.06.21.

1. Introduction

The infrared (IR) photodetectors with upper-limit performance regime limited only by the background radiation fluctuations [1, 2] today are mostly based on cooled to T ~ 78 K HgCdTe narrow-gap semiconductors. It was shown that at the same time the HgCdTe cooled and uncooled photoconductors can operate both in the IR and THz spectral ranges [3, 4]. The sensitivity in the THz range of these photoconductors is related with the electron gas heating under the THz radiation [5].

Relatively recently, it was shown that the optical polarization orientation in the THz range in zero-biased HgCdTe-based heterostructures is accompanied by the generation of a spin-dependent electrical current. In these objects with the zinc-blende structure (noncentro-symmetrical semiconductor, space group $\bar{4}3m\left(T_d^2\right)$, point group $\bar{4}3m\left(T_d\right)$), these effects were demonstrated in quantum wells (QWs) [6–8]. This is a result of displaying a non-equilibrium spin polarization of electrons and excitation of spin currents (like to that in spintronics objects) by a driving electric field of an electromagnetic wave. Spintronics is related with the spin data transfer in solid-state crystals or devices in addition to currents associated with the ordinary electronic charge.

Arising constant electromotive forces (unbiased samples, which are irradiated by circularly or linear polarized radiation) demonstrate sources of currents that are induced by polarized light. The electromotive force (emf) is not related to the spatial inhomogeneity of the irradiation or the inhomogeneity of the medium, and has been studied earlier (see, *e.g.*, [9, 10]). These effects represent a conversion of the angular moments of photons in polarized THz radiation into a translation motion of free carriers. In all these investigated QWs, there was no bias applied to the samples with relatively large area (~5×5 mm), in which the Airy disk area of the radiation beam is within the samples area.

The aim of this investigation is related with studying the possibility of the manifestation of the emf caused by spin currents in biased thin HgCdTe films antenna-coupled noncentro-symmetrical $Hg_{1-x}Cd_xTe$ photoconductors. These semiconductors have large spin-orbit coupling and that seems to be the base of emergence of additional spin-dependent signals, when being irradiated with linear or circular polarized THz radiation, in addition to orddinary currents associated with the electronic charge.

2. Rashba spin-splitting in noncentro-symmetrical semiconductors without magnetic field

Two types of spin splitting in zero magnetic fields are mainly found in semiconductors [11, 12], namely: the Rashba spin-splitting and the Dresselhaus one, which arise from structure inversion asymmetry and bulk inversion asymmetry [8, 13]. The Rashba spin-splitting generally occurs due to the spatial inhomogeneity at the interface or surface [13, 14], which can be governed by an external electric fields and strain. The Rashba effect is dominant in narrow-gap semiconductors [15] and attracts attention due to its possible tunability by an external electric field.

HgTe-CdTe binary phase diagram demonstrate full solubility at any x-values in $Hg_{1-x}Cd_xTe$ solid-state solutions [16]. Both HgTe and CdTe have the identical zinc blende type crystal structure, since both Hg and Cd are in the same group with a similar electronic configuration. Therefore, the solubility of $Hg_{1-x}Cd_xTe$ is high from $x = 0$ to $x = 1$ without undergoing any structural phase transition. These $Hg_{1-x}Cd_xTe$ solid-state solutions have large spin-orbit interaction. Band inversion occurs near the critical composition $x \approx 0.165$ where the band gap is zero. At $x > 0.165$, these solid-state solutions are semiconductors and have the ordinary direct band-gap E_g (see the left part of Fig. 1) between Γ_6 s-like conduction band and p-like Γ_8 valence bands. At $x < 0.165$, they have the inverted ("negative") band gap (right part of Fig. 1) and are semimetals.

The spin-orbit interaction originates from the **k·p**-mixing of the states in the conduction band and the states in the valence bands (**k·p**-theory requires only four spin-split bands: the three p-like Γ_7 and Γ_8 valence bands and the lowest Γ_6 s-like conduction band). The conduction electron states are strongly mixed with the valence states through the **k·p**-interaction across a narrow energy gap. This interaction is strong in narrow-gap HgCdTe semiconductors and lead to large values of the electron g-factors [17, 18]. In the investigated $Hg_{0.799}Cd_{0.0.201}Te$ semiconductor samples at $T = 80$ K g-factor $g(k = 0) \approx -130$.

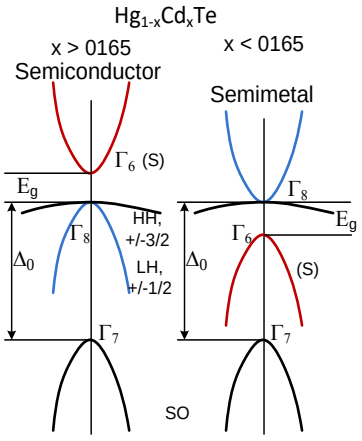

Fig. 1. Schematic band structure of $Hg_{1-x}Cd_xTe$ solid-state solutions. S is the conduction band, HH is the heavy-holes band, LH is the light-holes bands, and SO is the spin-orbit band.

Bulk HgCdTe solid-state solutions with a zinc blende lattice are nongyrotropic (the crystal class T_d), and, *e.g.*, circular photogalvanic effect (CPGE) due to current induced spin polarization (CISP) is forbidden in them. However, any external action such as a strain or external constant electric field, which reduces the crystal symmetry, leads to CISP for conduction electrons. The Rashba splitting arises in bulk semiconductors in an external electric field, because this field removes the center of spatial inversion. Since the intrinsic spin-orbit interaction in narrow-gap HgCdTe is strong, so pronounced should be the Rashba effect (momentum-dependent splitting of spin bands) as compared to other semiconductors.

In crystals with a high symmetry axis, the term with the spin-orbit interaction of electron in the conduction band in the Hamiltonian has the form [19]

$$H_{SO} = \alpha_R \cdot \boldsymbol{\sigma}_1 \times \mathbf{k}\boldsymbol{\nu}, \tag{1}$$

where α_R is the coefficient defining the value of spin-orbit interaction, $\boldsymbol{\sigma}$ are the Pauli matrices, $\mathbf{k}$ is the wave vector, and $\boldsymbol{\nu}$ is the unit vector. The H_{SO} lifts the two-fold spin degeneracy at $\mathbf{k} \neq 0$ and determines the spin-orbit splitting near $\mathbf{k} = 0$. The Rashba splitting in semiconductors with parabolic dispersion law can be fitted by the pair of the bands

$$E_{\pm} = \hbar^2 k^2 / 2m^* \pm \alpha_R \cdot k, \tag{2}$$

where m^* is the effective electron mass. In semiconductors with non-parabolic dispersion law the physical meaning of the Rashba splitting is not changed.

In a semiconductor placed into static electric filed E (interface or external), which withdraw the center of crystal space inversion and downgrade the system symmetry, the Rashba Hamiltonian of the spin-orbit interaction is as follows [20]:

$$H_{eff} = \xi_{SO} \cdot q \cdot [\boldsymbol{\sigma} \times \mathbf{k}] \cdot \mathbf{E}, \tag{3}$$

where q is the electron charge, $\boldsymbol{\sigma}$ are the Pauli matrices, $\mathbf{k}$ – wave vector, and $\mathbf{E}$ – electric field. The material-specific coefficient ξ_{SO} is the spin-orbit coupling parameter defining the Rashba spin-splitting energy. It depends on the momentum matrix element and the band-gap in narrow-gap semiconductor [21, 22]:

$$\xi_{SO} = \frac{P_0^2}{3} \times \frac{\Delta_0 \cdot (2E_g + \Delta_0)}{E_g^2 (E_g + \Delta_0)^2}, \tag{4}$$

where P_0 is the interband momentum matrix element, E_g is the band-gap (the separation between the Γ_6-conduction band and Γ_8-valence band edges), Δ_0 is the energy of spin-orbit splitting (the separation between the Γ_8-valence band and Γ_7-valence band edges).

For GaAs, where the spin-orbit splitting is small, the estimations give $\xi_{SO} \approx 5 \cdot 10^{-20}$ m^2, and ξ_{SO}(InSb) $\approx 5.5 \cdot 10^{-18}$ m^2, $\xi_{SO}(Hg_{0.799}Cd_{0.0.201}Te) \approx 3.3 \cdot 10^{-17}$ m^2 ($P_0 = 8.3 \cdot 10^{-8}$ eV·cm). Therewith, the influence of a constant electric field on the current-induced spin polarization and, therefore, CPGE and also linear photogalvanic effect (LPGE) should be pronounced in the taken for research *n*-type $Hg_{0.799}Cd_{0.201}Te$ semiconductor ($E_g \approx 0.084$ eV at $T = 80$ K) with the band-gap close to the critical point even in low-strength electric fields but under powerful circularly or linear polarized THz radiation.

The estimated values of $\xi_{SO} \cdot q \cdot E \approx (1.4…2.2) \cdot 10^{-13}$ eV·m in $Hg_{0.799}Cd_{0.201}Te$ in the typical low electric fields $(4.5…7) \cdot 10^3$ V/m. These electric fields were used in the below-indicated experiments. The values of $\xi_{SO} \cdot q \cdot E$ are smaller than the typical Rashba spin-splitting parameters $\alpha_R = 8.1 \cdot 10^{-12}$ eV·m and $\alpha_R = (4…7) \cdot 10^{-12}$ eV·m in AlGaN/GaN and InGaAs/InAlAs 2D heterostructures, respectively [23, 24]. In spite of the relatively small values of the ($\xi_{SO} \cdot q \cdot E$) coefficient, it happened to observe the influence of spin-orbit effects on the sensitivity of relatively long (several microns) narrow-gap photoconductors under powerful THz radiation. The response signals follow the temporal structure of a laser pulse, and the THz signal decay time was of the order of the pulse relaxation time $\tau \sim 75$ ns. Without antennas, the distances between the antennas edges were from 10 to 18 μm.

The $Hg_{1-x}Cd_xTe$ ($x \approx 0.201$) thin layers grown on the (013) GaAs substrate by using the molecular beam epitaxy (MBE) method were used [25]. The deviations of GaAs surface plane (013) orientation from the crystallographic axes were 1°…3° and for ZnTe/CdTe buffer layers – up to 8° [26]. The thickness of layers with the composition $x \approx 0.201$, in which photoresponse to THz radiation was observed, was $d \approx 2.4$ μm. The photoresponse was studied under radiation normally incident onto (013) grown films. The bow-tie and spiral antennas with dimensions $l \sim 1.5$ mm to input the THz radiation power were applied.

The curcuilar and linear THz radiation from gas lasers were used at the wavelength 280 μm ($h\nu \approx 0.0044$ eV) and 496 μm ($h\nu = 0.0025$ eV), which are much lower as compared to band-gap of $Hg_{0.799}Cd_{0.0.201}Te$ semiconductor. The circuilar and linear THz radiation from linearly polarized laser beam were obtained using λ/4 or λ/2-plates made from *x*-cut crystalline quartz. Linearly polarized radiation from lasers used to get a rotating linear polarized radiation was provided by a rotating λ/2-plate. The initial linearly polarized laser light was transferred into circularly, elliptically, and linearly polarized radiations that were provided by a rotating λ/4-plate (see, *e.g.*, [27]). The radiation spot diameter was about 1.5…2.5 mm, depending on the radiation frequency. The peak intensity of the THz laser power was of the order of $P \approx 10$ kW and was controlled with a fast room-temperature pyroelectric detector. As well, the pulse shape and the spatial distribution of the laser radiation have been measured and showed an almost Gaussian profile [28].

3. Experimental

The observed oscillograms of HgCdTe photoconductors grown on (013) GaAs substrates with bow-tie and spiral antennas to circularly or linearly polarized radiation are rather similar and depend on direction of a constant electric field applied to bias photoconductors and the state of polarization of the THz radiation.

For the elliptically and linearly polarized states of laser pulse radiation and in the case of applied electrical field *E* biases, except the ordinary response related with absorption by free carriers ($h\nu < E_g$, where E_g is the band-gap), there was observed an additional photoresponse with a complicated form of dependences on the polarization angles (see Figs 2 and 3). This may indicate contribution of additional mechanisms to the resulting photoresponse signals related with the photogalvanic (PGE) (electronic current arises, when radiation falls down onto semiconductor) and the photon drag effects (PDE) [29].

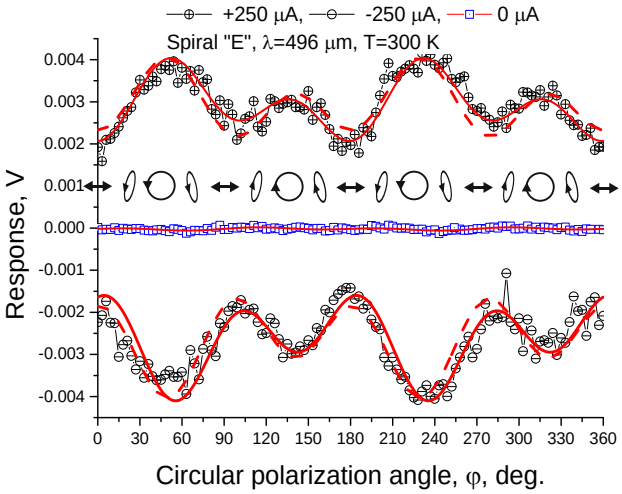

Fig. 2. Photoresponse signals of MCT HEB with spiral antenna (sample "E") as a function of the laser radiation helicity (λ = 496 μm) measured at room temperature in the sample with ohmic contacts, when no Schotky barrier fields arise. The laser circular polarization conditions are sketched according to the phase angle φ (the angle φ defines rotation of the *c*-axis in the λ/4 plate with respect to the initial linear laser polarization plane). Measurements (symbols) were carried out at biases with opposite signs. Dashed curves are the fits by Eq. (6) (see below). The fitting parameters are as follows: for the temperature $T = 300$ K (I_{bias} =+250 μA) $U_0 = 0.00295$, $U_{circ} = 2.2823 \cdot 10^{-4}$, $U_{L1} = -2.5908 \cdot 10^{-4}$, $U_{L2} = -0.00061$, V; (I_{bias} = –250 μA) $U_0 = -0.00267$, $U_{circ} = -1.94954 \cdot 10^{-4}$, $U_{L1} = 0.919565 \cdot 10^{-4}$, $U_{L2} = 3.99045 \cdot 10^{-4}$, V. Solid lines show the fitting when the polarization angle φ in Eq. (7) is shifted by 18°, which is related with orientation of (013) plane of the investigated sample. The fitting parameters: for T=300 K (I_{bias} = +250 μA) $U_0 = 0.00295$, $U_{circ} = 5.50345 \cdot 10^{-4}$, $U_{L1} = -0.00128$, $U_{L2} = -1.3753 \cdot 10^{-4}$, V; ($I_{bias}$= –250 μA) $U_0 = -0.00268$, $U_{circ} = -6.06522 \cdot 10^{-4}$, $U_{L1} = 0.00254$, $U_{L2} = 0.00116$, V.

Table. The fitting parameters for Fig. 3 with the use of Eq. (5).

Fitting parameters	Bias current I_{bias}, μA						
	–400	–300	–200	0	200	300	400
U'_0, V	$-4.399\cdot10^{-4}$	$-3.297\cdot10^{-4}$	$-2.108\cdot10^{-4}$	$-2.31\cdot10^{-5}$	$1.740\cdot10^{-4}$	$2.620\cdot10^{-4}$	$4.207\cdot10^{-4}$
U'_{L1}, V	$6.741\cdot10^{-5}$	$6.514\cdot10^{-5}$	$4.182\cdot10^{-5}$	$5.072\cdot10^{-7}$	$-5\cdot10^{-5}$	$-5.833\cdot10^{-5}$	$-7.906\cdot10^{-5}$
U'_{L2}, V	$-1.696\cdot10^{-4}$	$-1.115\cdot10^{-4}$	$-8.493\cdot10^{-5}$	$-1.53\cdot10^{-5}$	$7.636\cdot10^{-6}$	$2.003\cdot10^{-5}$	$1.511\cdot10^{-4}$

For linear polarized radiation, the angle dependent photoresponse can be well described by the following expression

$$U_{resp}^{Lin} = U'_0 + U'_{L1}\cdot\cos 2\alpha + U'_{L2}\cdot\sin 2\alpha\,. \qquad (5)$$

Here, $P_{L1} = \cos 2\alpha$ and $P_{L2} = \sin 2\alpha$ are the Stokes parameters for linearly polarized radiation passing through the λ/2-plate with different weights given by the fit coefficients U'_{L1}, U'_{L2}, and U'_0. The angle α is the angle between the *c*-axis (fast direction) of the λ/2-plate for the plane with linearly polarized radiation and the plane of linearly polarized radiation at the output of the λ/2-plate.

In the case of circularly polarized radiation, the overall polarization dependent response signals U_{resp} in the systems with reduced symmetry can be fitted by the expression [30]:

$$U_{resp} = U_0 + U_{circ}\sin(2\varphi) + U_{L1}\frac{\cos(4\varphi)+1}{2} + U_{L2}\cdot\frac{\sin(4\varphi)}{2}. \qquad (6)$$

Here, the Stokes parameters defining the degree of linear polarization in the elliptically polarized radiation are varied as [30]

$$P_{L1} = \frac{\cos(4\varphi)+1}{2},\quad P_{L2} = \frac{\sin(4\varphi)}{2} \qquad (7)$$

and the degree of circular polarization P_{circ} of the elliptically polarized radiation after passing the λ/4-plate is changed according to [27]

$$P_{circ} = \frac{I^{\sigma+} - I^{\sigma-}}{I^{\sigma+} + I^{\sigma-}} = \sin(2\varphi). \qquad (8)$$

In the case of circularly polarized radiation, the weight coefficients U_{L1}, U_{L2}, U_{circ}, and U_0 are the fit coefficients used in fitting procedure.

The results shown in Figs 2 and 3 were obtained for the samples with Ohmic contacts. The curves with inverted biases are almost symmetrical but have different signs. Without applying the constant electric field, there observed are almost no signals. But when the contacts are not Ohmic, there observed are the signals even at $E = 0$ (Fig. 4), which seems to be related to the internal electric field of Schottky barriers.

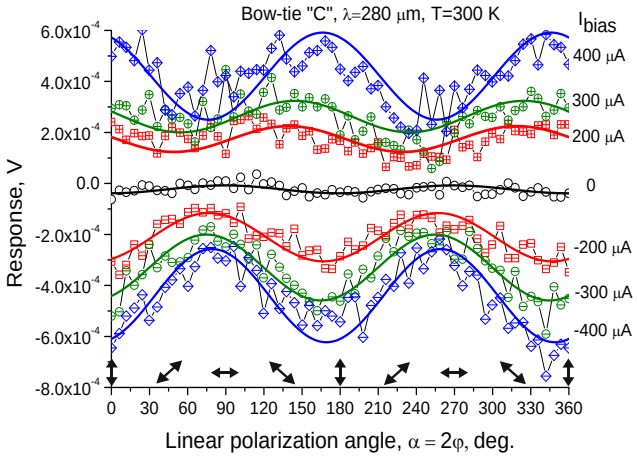

Fig. 3. The room-temperature dependences of measured photoresponse signals of MCT HEBs with bow-tie antennas on the linear polarization angle α = 2φ, where φ is the angle between the optical axes of a λ/2 plate and the initial linear polarization direction (initial plane of linear polarization). The measurements (symbols) were carried out at different bias currents under the pulsed-laser radiation at λ = 280 μm, R_{300K} = 192 Ohm. After the λ/2-plate, the angle of rotation of a linear polarized radiation α = 2φ. The fitting parameters for cutves in this figure are shown in Table.

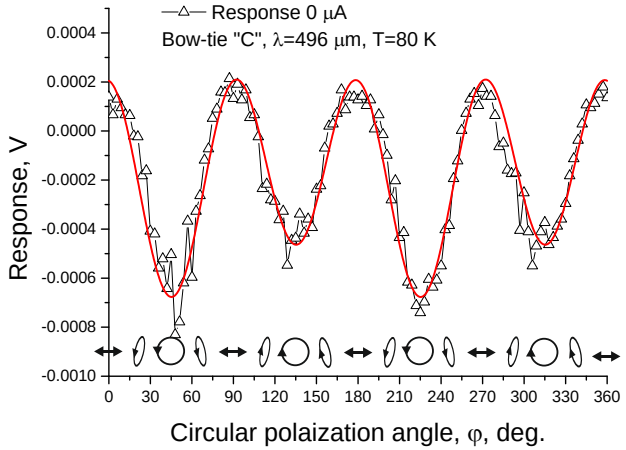

Fig. 4. The photoresponse signal of HgCdTe photoconductor with bow-tie antenna with non-Ohmic contacts at zero bias as a function of the laser radiation helicity (λ= 496 μm) measured at T = 80 K. The laser elliptically polarization conditions are sketched according to the key phase angle φ. The solid curve is the fit by using Eq. (6) with parameters $U_0 = -1.82625\cdot10^{-4}$, $U_{circ} = -0.53269\cdot10^{-4}$, $U_{L1} = 3{,}586325\cdot10^{-4}$, $U_{L2} = 3.05522\cdot10^{-4}$, V.

4. Conclusions

The polarization-dependent responses in epitaxial layers of the noncentro-symmetrical HgCdTe and non-magnetic photoconductors having the large spin-orbit coupling have been studied. They show the spin-polarization dependent sensitivity in the THz range related with absorption by free carriers at T = 80 and 300 K. The polarization-dependent photoresponse is related with breaking the symmetry of photoconductive HgCdTe films under action of an external constant electric field (or internal Schottky barrier electric field), which results in the polarization-sensitive photogalvanic spin transport electronics (spintronics) phenomena without applying any external magnetic field.

Acknowledgments

This work was partly supported by the Volkswagen Foundation Partnerships-Cooperation Project No. 97738 "Terahertz optoelectronics in novel low-dimensional narrow-gap semiconductor nanostructures" and the NAS of Ukraine, project No. 20/1-P. S.N. Danilov gratefully acknowledges the support of the Deutsche Forschungsgemeinschaft (DFG) – Project-ID 314695032-SFB 1277 and the Elite 253 Network of Bavaria (K-NW-2013-247).

References

1. Rogalski A. *Infrared Detectors*. CRC Press, Boca Raton, 2011.
2. Kinch M.A. *State-of-the-Art Infrared Detector Technology*. SPIE Press Book, Bellingham, 2014. https://doi.org/10.1117/3.2072367.
3. Sizov F., Zabudsky V., Dvoretskii S. *et al*. Two-color detector: Mercury-cadmium-telluride as a terahertz and infrared detector. *Appl. Phys. Lett.* 2015. **106**. P. 082104. https://doi.org/10.1063/1.4913590.
4. Zabudsky V., Sizov F., Momot N. *et al*. THz/sub-THz direct detection detector on the basis of electron/hole heating in MCT layers. *Semicond. Sci. Technol.* 2012. **27**, No 4. P. 045002. https://doi.org/10.1088/0268-1242/27/4/045002.
5. Dobrovolsky V., Sizov F. THz/sub-THz bolometer based on electron heating in a semiconductor waveguide. *Opto-Electron. Rev*. 2010. **18**. P. 250–258. https://doi.org/10.2478/s11772-010-1033-8.
6. Danilov S.N., Wittmann B., Olbrich P. Fast detector of the ellipticity of infrared and terahertz radiation based on HgTe quantum well structures. *J. Appl. Phys*. 2009. **105**. P. 013106. https://doi.org/10.1063/1.3056393.
7. Olbrich P., Zoth C., Vierling P. *et al*. Giant photocurrents in a Dirac fermion system at cyclotron resonance. *Phys. Rev. B*. 2013. **87**, Issue 23. P. 235439. https://doi.org/10.1103/PhysRevB.87.235439.
8. Ivchenko E.L. and Ganichev S.D. *Spin Photogalvanics*. M.I. Dyakonov (Ed.). *Spin Physics in Semiconductors.* Berlin, Springer, 2017. https://doi.org/10.1007/978-3-319-65436-2.
9. Ganichev S.D., Ivchenko E.L., Bel'kov V.V. *et al*. Spin-galvanic effect. *Nature.* 2002. **417**(6885). P. 153–156. https://doi.org/10.1038/417153a.
10. Ivchenko E.L., Pikus G.E. *Superlattices and other Heterostructures: Symmetry and Optical Phenomena.* Berlin, Springer, 1995.
11. Bychkov Y.A., Rashba E.I. Oscillatory effects and the magnetic susceptibility of carriers in inversion layers. *J. Phys. C: Solid State Phys.* 1984. **17**(33). P. 6039. https://doi.org/10.1088/0022-3719/17/33/015.
12. Dresselhaus G. Spin-orbit coupling effects in zinc blende structures. *Phys. Rev. B.* 1955. **100**. P. 580. https://doi.org/10.1103/PhysRev.100.580.
13. Ganichev S.D., Golub L.E. Interplay of Rashba/Dresselhaus spin splittings probed by photogalvanic spectroscopy – A review. *phys. status solidi b.* 2014. **251**. P. 1801. https://doi.org/10.1002/pssb.201350261.
14. Stein D., Klitzing K., Weimann G. Electron spin resonance on GaAs–$Al_xGa_{1-x}As$ heterostructures. *Phys. Rev. Lett.* 1983. **51**. P. 130. https://doi.org/10.1103/PhysRevLett.51.130.
15. Lommer G., Malcher F., Rossler U. Spin splitting in semiconductor heterostructures for $B\rightarrow 0$. *Phys. Rev. Lett.* 1988. **60**. P. 728. https://doi.org/10.1103/PhysRevLett.60.728.
16. *Mercury Cadmium Telluride: Growth, Properties and Applications*. P. Capper, J. Garland (Eds.). Wiley, 2010.
17. Litvinenko K.L., Nikzad L., Pidgeon C.R. *et al*. Temperature dependence of the electron Landé g factor in InSb and GaAs. *Phys. Rev. B.* 2008. **77**. P. 033204. https://doi.org/10.1103/PhysRevB.77.033204.
18. Kim R.S., Narita S. Far-infrared interband magneto-absorption and band structure of $Hg_{1-x}Cd_xTe$ alloys. *phys. status solidi b.* 1976. **73**. P. 741. https://doi.org/10.1002/pssb.2220730244.
19. Bychkov Yu.A., Rashba E.I. Properties of a 2D electron gas with lifted spectral degeneracy. *JETP Lett.* 1984. **39**, Issue 2. P. 78–81.
20. Barnes S.E., Ieda J., Maekawa S. Rashba spin-orbit anisotropy and the electric field control of magnetism. *Sci. Rep.* 2014. **4**. P. 4105. https://doi.org/10.1038/srep04105.
21. Radantsev V.F., Yafyasov A.M. Rashba splitting in MIS structures HgCdTe. *J. Exp. Theor. Phys.* 2002. **95**. P. 491–501. https://doi.org/10.1134/1.1513822.
22. Winkler R. *Spin-Orbit Coupling Effects in Two-Dimensional Electron and Hole Systems*. Springer Tracts in Modern Physics. **191**. Springer, 2003. https://doi.org/10.1007/b13586.
23. Morrison C., Wiśniewski P., Rhead S.D. *et al*. Observation of Rashba zero-field spin splitting in a strained germanium 2D hole gas. *Appl. Phys. Lett.* 2014. **105**. P. 182401. https://doi.org/10.1063/1.4901107.
24. Yao Q., Cai J., Tong W. *et al.* Manipulation of the large Rashba spin splitting in polar two-dimensional

transition-metal dichalcogenides. *Phys. Rev. B.* 2017. **95**. P. 165401. https://doi.org/10.1103/PhysRevB.95.165401.
25. Dvoretsky S.A., Mikhailov N.N., Remesnik V.G. *et al*. MBE-grown MCT hetero- and nanostructures for IR and THz detectors. *Opto-Electron. Rev.* 2019. **27**. P. 282–290. https://doi.org/10.1016/j.opelre.2019.07.002.
26. Stupak M.F., Mikhailov N.N., Dvoretskii S.A. *et al.* Possibilities of characterizing the crystal parameters of $Cd_xHg_{1-x}Te$ structures on GaAs substrates by the method of generation of the probe-radiation second harmonic in reflection geometry. *Phys. Solid State*. 2020. **62**. P. 252–259. https://doi.org/10.1134/S1063783420020201.
27. Hubmann S., Budkin G.V., Otteneder M. *et al*. Symmetry breaking and circular photogalvanic effect in epitaxial $Cd_xHg_{1-x}Te$ films. *Phys. Rev. Materials*. 2010. **4**. P. 043607. https://doi.org/10.1103/PhysRevMaterials.4.043607
28. Bel'kov V.V., Ganichev S.D., Schneider P. *et al*. Circular photogalvanic effect at inter-band excitation in semiconductor quantum wells. *Solid State Commun.* 2003. **128**. P. 283–286. https://doi.org/10.1016/j.ssc.2003.08.022.
29. Shalygin V.A., Moldavskaya M.D., Danilov S.N. *et al.* Circular photon drag effect in bulk tellurium. *Phys. Rev. B.* 2016. **93**. P. 045207. https://doi.org/10.1103/PhysRevB.93.045207.
30. Bel'kov V.V., Ganichev S.D., Ivchenko E.L. *et al*. Magneto-gyrotropic photogalvanic effects in semiconductor quantum wells *J. Phys. Cond. Matt.* 2005. **17**. P. 3405. https://doi.org/10.1088/0953-8984/17/21/032.

Authors and CV

Zinoviia Tsybrii is the head of the Laboratory at the V. Lashkaryov Institute of Semiconductor Physics, NAS of Ukraine. She received the PhD degree in 2000. Her current research interests include physics of semiconductors, IR and THz detectors manufacturing and investigation.

Sergey Danilov received the PhD degree from the St.-Petersburg State Polytechnic University in 1999. Since 2002, he has been a Research Fellow at the Terahertz Center, University of Regensburg, Germany. His research interests include semiconductor physics, nanoelectronics, phenomena under IR, THz excitation.

Joanna Gumenjuk-Sichevska received her PhD degree from V. Lashkaryov Institute of Semiconductor Physics, NASU in 1991, currently she is Senior Researcher at the same institute. Her research interests include transport and optical properties of low-dimensional structures, optoelectronics in a field of IR and THz photodetectors.

Nikolai Mikhailov received the PhD degree from Rzhanov Institute of Semiconductor Physics of the Siberian Branch of the RAS in 2005. The area of scientific interests is the growth of II-VI compound including narrow gap HgCdTe hetero- and nanostructures by molecular beam epitaxy.

Sergey Dvoretskii received the PhD degree from Rzhanov Institute of Semiconductor Physics of the Siberian Branch of the RAS in 1975. Now he is the head of the department of infrared optoelectronic devices based on MCT. His research interests are the growth II-VI compound including HgCdTe hetero- and nanostructures.

Evgen Melezhik is researcher at the V. Lashkaryov Institute of Semiconductor Physics, NAS of Ukraine. He received the PhD degree in 2016. His research interests include numerical modeling of band structure and electronic transport properties of low-dimensional HgCdTe compounds for the needs of THz electronics.

F. Sizov, Doctor of Sciences in Physics and Mathematics, Professor, Corresponding Member of NAS of Ukraine, Head of Department at the V. Lashkaryov Institute of Semiconductor Physics, NAS of Ukraine. He is the Fellow SPIE member and EuMA member. His area of scientific interests includes physics of semi-conductors, low-dimensional semiconductor systems, IR and THz physics.

Явища спінтроніки, індуковані ТГц випромінюванням, у вузькощілинних тонких плівках HgCdTe у зовнішньому постійному електричному полі

З.Ф. Цибрій, С.Н. Данилов, Ж.В. Гуменюк-Сичевська, Н.Н. Михайлов, С.А. Дворецкий, Є.О. Мележик, Ф.Ф. Сизов

Анотація. Досліджено відгук неохолоджуваних (T = 300 K) та охолоджуваних до T = 78 K інтегрованих з антеною тонкоплівкових фотопровідників на основі вузькощілинного $Hg_{1-x}Cd_xTe$, що мають велику спін-орбітальну взаємодію і опромінених терагерцовим (ТГц) випромінюванням (лінійно або циркулярно поляризованим). Потужне ТГц випромінювання спричиняє фотоструми, знак та величина яких контролюються орієнтацією осей антен, напрямком зовнішнього постійного електричного поля та орієнтацією електричного поля поляризованого випромінювання (циркулярного або лінійного), що падає на фотопровідники. Спостережувані ефекти, можливо, зумовлено спіновими струмами, що властиві пристроям, в яких виявляються спінтронні ефекти.

Ключові слова: спінтронні явища, фотопровідники, ТГц випромінювання, HgCdTe.